Computers and Geotechnics 164 (2023) 105834

Contents lists available at ScienceDirect

Computers and Geotechnics

journal homepage: www.elsevier.com/locate/compgeo

Symbolic algebra integration of soil elastoplastic models

Vicente Navarro [a,*], Arianna Pucci [b], Erik Tengblad [a], Francesca Casini [b], Laura Asensio [a]

[a] Geoenvironmental Group, Universidad de Castilla-La Mancha, Avda. Camilo José Cela 2, 13071 Ciudad Real, Spain
[b] Dipartimento di Ingegneria Civile e Ingegneria Informatica (DICII) Universita' degli Studi di Roma Tor Vergata, Italy

ARTICLE INFO

Keywords:
Elastoplastic models
Symbolic algebra
Time integration

ABSTRACT

This work analyses the time integration of elastoplastic models using implementation platforms with symbolic algebra capabilities. In such platforms, the variables and state functions involved in solving boundary value problems are considered entities continuous in time, thus the time integration of stresses and hardening parameters is always based on implicit schemes. The latter confers to the computation an accuracy that is inspected in this work by analysing the integration of the Clay and Sand Model. Finally, the advantages of using integration schemes in which the linearisation of the yield function is imposed to be zero when calculating the plastic multiplier are illustrated.

1. Introduction

The application of symbolic differentiation techniques (Martins and Hwang, 2013) in numerical models allows obtaining a high-quality system iteration matrix, which substantially improves the numerical performance of the model (Gobbert et al., 2009). Thus, the use of implementation platforms that incorporate symbolic algebra capabilities is a promising approach to the advancement of computational modelling in geotechnical analysis. On such platforms, as when using numerical tools that do not incorporate symbolic algebra, the solution for any time is approximated by a discrete number of georeferenced functions according to the chosen spatial discretisation strategy. When using symbolic algebra, however, these functions are considered entities continuous in time. This gives the time integration of the constitutive models special characteristics that must be analysed to better understand the implications for the characterisation of the mechanical behaviour of the system. This is the aim of this paper. First, the integration by means of symbolic algebra of a wide family of elastoplastic models is analysed. An integration strategy is presented that is based on the adaptation of the scheme presented by Halilovič et al. (2009, 2017). After that, as an example, the strategy is particularised for the Clay And Sand Model (CASM) of (Yu, 1998). To conclude, an inspection exercise is presented to illustrate the scope of the proposal.

2. Integration of elastoplastic models using symbolic algebra

This work adopts a classical approach to plasticity, defined with the yield function, the hardening law and the flow rule. For an internal organisation of the soil characterised by the vector of hardening parameters χ (vectors and tensors are denoted in bold), the mechanical behaviour of the soil is elastic if the value of the yield function F is negative for the current constitutive stress σ (stress and strain are expressed as vectors using Voigt notation)

$$F(\boldsymbol{\sigma},\boldsymbol{\chi}) < 0 \tag{1}$$

When F becomes equal to 0, the applied stress reaches the limit withstood by the existing organisation. The soil restructures plastically, producing an increment of χ defined by the hardening law

$$d\boldsymbol{\chi} = \frac{\partial \boldsymbol{\chi}}{\partial \boldsymbol{\varepsilon}_p} \cdot d\boldsymbol{\varepsilon}_p \tag{2}$$

where the plastic strain $d\varepsilon_p$ is calculated with the flow rule as a function of the plastic multiplier $d\lambda$ and the plastic vector $\mathbf{n}$

$$d\boldsymbol{\varepsilon}_p = d\lambda \cdot \boldsymbol{n} \tag{3}$$

$\mathbf{n}$ is usually computed as the gradient of the plastic potential Q (equal to F in associated plasticity models)

$$\boldsymbol{n} = \frac{\partial Q}{\partial \boldsymbol{\sigma}} \tag{4}$$

It is further assumed that, with or without plastic behaviour, the elastic matrix $\mathbf{D}$ enables the constitutive stress increment to be computed as a

* Corresponding author.
E-mail address: Vicente.Navarro@uclm.es (V. Navarro).

https://doi.org/10.1016/j.compgeo.2023.105834
Received 18 September 2023; Received in revised form 27 September 2023; Accepted 28 September 2023
Available online 1 October 2023

function of the elastic strain increment $d\varepsilon_e$

$$d\sigma = D \cdot d\varepsilon_e \tag{5}$$

In plastic stress paths, Eqs. (2) and (5) must be integrated in time to characterise the evolution of the system. To do so, the plastic multiplier needs to be known. It is usually obtained by applying the consistency condition derived by assuming $dF = 0$: if F is always null in a plastic path, so is dF. Therefore, from Eqs. (2), (3) and (5) it follows that

$$dF = \frac{\partial F}{\partial \boldsymbol{\sigma}} \cdot d\boldsymbol{\sigma} + \frac{\partial F}{\partial \chi} \cdot d\chi = 0 \rightarrow d\lambda = \frac{1}{H_p} \frac{\partial F}{\partial \boldsymbol{\sigma}} \cdot \boldsymbol{D} \cdot d\boldsymbol{\varepsilon} \tag{6}$$

where the plastic hardening modulus H_p is computed as

$$H_p = \left(\frac{\partial F}{\partial \boldsymbol{\sigma}} \boldsymbol{D} - \frac{\partial F}{\partial \chi} \frac{\partial \chi}{\partial \boldsymbol{\varepsilon}_p} \right) \cdot \boldsymbol{n} \tag{7}$$

When deriving Eq. (6), the total strain $d\varepsilon$ was assumed to fulfil the following

$$d\boldsymbol{\varepsilon} = d\boldsymbol{\varepsilon}_e + d\boldsymbol{\varepsilon}_p \tag{8}$$

It is accepted that the soil experiences only the elastic strain $d\varepsilon_e$ caused by changes in the constitutive stress σ and the plastic strain $d\varepsilon_p$ resulting from the rearrangement that takes place when $F = 0$. If other types of strains $d\varepsilon^*$ occurred, such as those caused by the microstructure in double porosity soils (Gens and Alonso, 1992), Eq. (8) should be written as

$$d\boldsymbol{\varepsilon} = d\boldsymbol{\varepsilon}_e + d\boldsymbol{\varepsilon}_p + d\boldsymbol{\varepsilon}^* \tag{9}$$

If, in addition, any magnitude × additional to the stress σ were to intervene in the definition of the yield function, as, for example, suction s in the Barcelona Basic Model (Alonso et al., 1990; Alonso et al., 1999; Vaunat et al., 2000), Eq. (6) should be written as

$$d\lambda = \frac{1}{H_p} \left(\frac{\partial F}{\partial \boldsymbol{\sigma}} \cdot \boldsymbol{D} \cdot (d\boldsymbol{\varepsilon} - d\boldsymbol{\varepsilon}^*) + \frac{\partial F}{\partial \boldsymbol{x}} d\boldsymbol{x} \right) \tag{10}$$

Eqs. (2) and (5) can be integrated with this value of the plastic multiplier. The magnitudes involved in the equations are a function of the variables to be integrated, σ and χ, which, as pointed out in the Introduction, are automatically updated functions thanks to symbolic algebra. Therefore, the calculation of stress and hardening parameters is a totally implicit problem. Consequently, it can be expected to show the accuracy of implicit integration schemes implemented in codes that do not incorporate symbolic algebra (Borja and Lee, 1990; Lloret-Cabot and Sheng, 2022).

Even if the implicit structure of Eq. (6) is promising, the expectations of good computational performance can be raised when taking into account the results obtained when the derivation of the plastic multiplier is based on the approximation of F and not of dF (Halilovič et al., 2009; 2017). Those authors show robust and accurate results without iterations, without additional integration substeps and without imposing any return mapping algorithm (for more information on this type of techniques, see, for example, (Potts and Gens, 1985; Gens and Potts, 1988). To do so, the first terms of the Taylor series development of F are taken and $F = 0$ is imposed. Operating analogously to the derivation of Eqs. (6) and (10) it results in

$$d\lambda = \frac{1}{H_p} \left(F + \frac{\partial F}{\partial \boldsymbol{\sigma}} \cdot \boldsymbol{D} \cdot (d\boldsymbol{\varepsilon} - d\boldsymbol{\varepsilon}^*) + \frac{\partial F}{\partial s} ds \right) \tag{11}$$

The only difference between Eq. (10) and Eq. (11) is the inclusion of F. The scheme remains fully implicit. Thus, unlike the explicit formulation proposed by Halilovič et al. (2009, 2017), the value of F in Eq. (11) is not obtained at the time prior to the computation time but is an updated value. In this sense, if Halilovič et al. (2009) label their method as "NICE" (Next Increment Corrects Error) because the error potentially made in one computational time step is corrected in the next one, the formulation proposed here should be called "CICE", since the symbolic algebra makes the potential integration drift to be corrected in the Current computational time. Therefore, the computational performance of the new proposed CICE will be better than that of NICE, which is already satisfactory.

3. Example of application. Inspection on the scope of the method

To analyse the scope of the method more clearly, saturated cases are analysed, with $d\varepsilon^* = \mathbf{0}$, in which the constitutive stresses σ will be the Terzaghi effective stresses. However, in order not to lose generality, a non-associated plasticity model is adopted, using the CASM as proposed by (Yu, 1998). In CASM, the vector of hardening parameters χ is the effective mean preconsolidation stress p_0. The hardening law in Eq. (2) is written as

$$dp_0 = \frac{(1+e)\, p_0}{\lambda - \kappa} d\varepsilon_p^V \tag{12}$$

where $d\varepsilon_p^V$ is the volumetric component of the plastic strain $d\varepsilon_p$, e is the total void ratio ($=V_V/V_S$, where V_V is the volume of voids and V_S is the solid mineral volume), and the material parameters λ and κ are, respectively, the slope of the virgin compression line and the elastic compressibility parameter (Table 1). The yield surface is defined as

$$F = \left(\frac{q}{M\, p} \right)^n + \frac{Ln(p/p_0)}{Ln\, r} \tag{13}$$

where q is the von Mises deviatoric stress, p is the effective mean stress, M is the slope of the critical state line (Table 1), n and r are material parameters that constrain the shape of the yield surface on the deviatoric plane (Table 1). The flow rule is given by dilatancy δ, taken from (Rowe, 1962)

$$\delta = \frac{d\varepsilon_p^V}{d\varepsilon_p^S} = \frac{9\left(M - \frac{q}{p}\right)}{9 + 3M - 2M\frac{q}{p}} \tag{14}$$

where $d\varepsilon_p^S$ is the plastic deviatoric strain. For the isotropic material under consideration, the elastic matrix expressed in terms of the stress terms p and q and their conjugate strains $d\varepsilon_e^V$ and $d\varepsilon_e^S$ are derived from the elastic matrix **D**

$$\boldsymbol{D} = \begin{bmatrix} K & 0 \\ 0 & 3G \end{bmatrix} \tag{15}$$

Bulk modulus K is computed as

$$K = \frac{(1+e)\, p}{\kappa} \tag{16}$$

and shear modulus G is computed as

$$G = \frac{3\,(1-2\,\nu)}{2\,(1+\nu)} K \tag{17}$$

ν is Poisson's ratio (Table 1). With Eq. (15), basing the integration of σ and p_0 on $d\varepsilon_p^S$ instead of $d\lambda$, from Eqs. (10), (12), (13) and (14) it follows

Table 1
Material parameters used in the simulations.

Parameter	Value	Relevant equation
Λ	0.093	(12)
K	0.025	(12)
M	0.733	(13)
ν	0.3	(17)
r	2.714	(13)
n	4.5	(13)

that

$$d\varepsilon_p^S = \frac{1}{H_p}\left(K\frac{\partial F}{\partial p}d\varepsilon^V + 3G\frac{\partial F}{\partial q}d\varepsilon^S\right) \quad (18)$$

The plastic hardening modulus is defined in this case as

$$H_p = \left(K\frac{\partial F}{\partial p} - \frac{\partial F}{\partial p_0}\right)\delta + 3G\frac{\partial F}{\partial q} \quad (19)$$

In turn, keeping this definition of H_p, from Eq. (12) it derives that

$$d\varepsilon_p^S = \frac{1}{H_p}\left(F + K\frac{\partial F}{\partial p}d\varepsilon^V + 3G\frac{\partial F}{\partial q}d\varepsilon^S\right) \quad (20)$$

$d\varepsilon_p^V$ is calculated with $d\varepsilon_p^S$ and Eq. (14). dp_0 is then obtained with Eq. (12).

Four conventional triaxial tests are simulated. In these tests, after an isotropic consolidation, an axial loading phase is performed at a constant displacement rate, keeping the cell pressure constant. The tests performed on some samples of remoulded Weald Clay (Liquid Limit = 43, Plastic Limit = 18) and presented by (Bishop and Henkel, 1957) are analysed. For each triaxial test (Table 2), whether drained (Figs. 1 and 2) or undrained (Figs. 3 and 4), two samples were tested: a normally consolidated one (overconsolidation ratio, OCR, = 1) and a heavily overconsolidated one (OCR = 24). The material parameters in Table 1, taken from (Yu, 1998), were used in the models.

Using Comsol Multiphysics (Comsol AB, 2018) as implementation platform, Eqs. (12) to (20) have been introduced in a computational module developed from the numerical model of (Navarro et al., 2019). The model, based on using the "multiphysics" capability of Comsol (Comsol AB, 2018) to make own developments without built-in modules, was extensively validated with a number of thermo-hydro-mechanical-chemical problems related to the behaviour of active soils (Navarro et al., 2017; 2022, 2023). The adoption of CICE makes the potential integration drift to be corrected in the Current computational time, which is the original contribution of this work.

Therefore, the simulations presented in the paragraphs below are based on the resolution of a boundary value problem, not on a Gaussian point level analysis. This gives greater scope to the inspection carried out, as the validity of the proposed algorithm is evaluated once it has been integrated into a finite element module. However, given the homogeneity of the specimens, initial conditions and boundary conditions in the solved problems, this scope has a certain limitation. Confidence in the proposed methodology will increase with increasing experience in its application to solve mechanical problems in more complex systems.

Figs. 1 and 2 plot a comparison of the experimental and modelled ε_z (vertical strain) - q and ε_z - ε_V (volumetric strain) paths, respectively, for a drained test on a normally consolidated and an overconsolidated samples. The model results plotted correspond to two formulations, which used, respectively, Eq. (18) (that is, Eq. (10)) and Eq. (20) (that is, Eq. (11)) as the base for integration. The results of both models (solutions with Eqs. (18) and (20)) are almost identical and overlap in the figure.

For the normally consolidated sample, both models satisfactorily

Table 2
Description of the modelled tests. Φ and H, diameter and height of the samples, respectively; e_0, initial void ratio; $p_{0\ ini}$, initial effective mean preconsolidation stress; p_{ini}, initial effective stress; Δt, test duration. D, drained test; U, undrained test; NC, normally consolidated sample (OCR = 1); OC, overconsolidated sample (OCR = 24).

Test ID	Φ (mm)	H (mm)	e_0	$p_{0\ ini}$ (kPa)	p_{0ni} *(kPa)*	Δt (h)
D-NC	35	70	0.632	207	207	30
U-NC						6
D-OC			0.617	828	34.5	23
U-OC						6

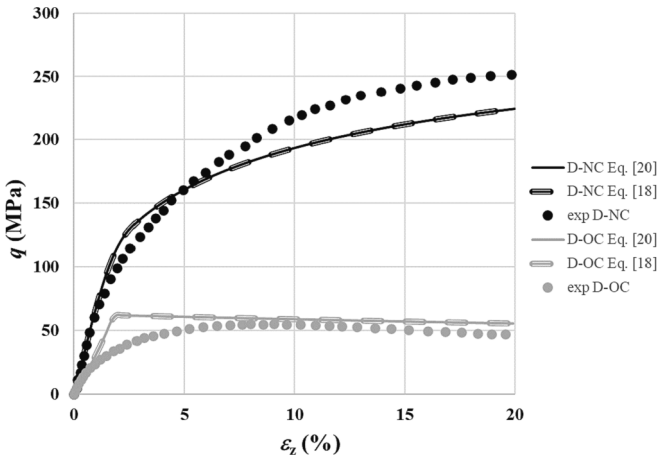

Fig. 1. Evolution of the axial strain ε_z and the von Mises stress q in the drained tests. In black, normally consolidated sample (OverConsolidation Ratio OCR = 1). In grey, heavily overconsolidated sample (OCR = 24). Markers, experimental data. Lines, model results.

reproduce the progressive hardening (Fig. 1) and contraction (Fig. 2) of the soil. The good quality of the results obtained with Eq. (18) makes that the improvement derived from using Eq. (20) is small.

To illustrate this fact more clearly, Fig. 5a shows the evolution throughout the simulations of the p_R / p_0 ratio. The reference effective mean stress p_R represents the value that p_0 should have in Eq. (13) for F to be zero for each (p, q) stress state. In the elastic regime, the ratio is less than 1, and it becomes equal to 1 in the plastic regime. Values greater than 1 indicate plastic drift. Fig. 5a shows the excellent values (zero drift) obtained with Eq. (20). Also, the values obtained with Eq. (18) with p_R / p_0 nearly equal to 1 are very satisfactory.

For the drained test on an overconsolidated sample, the comparison is similar. Eqs. (18) and (20) reproduce the same peak stress (Fig. 1) and the same dilatant behaviour (Fig. 2). In this case, Fig. 5b represents the obtained p_R / p_0 after yield, because its initial value for an overconsolidation ratio of 24 (Table 2) is very small, which would make the scale less clear for comparison.

Analogous results are obtained for the undrained tests. Eqs. (18) and (20) satisfactorily reproduce the water pressure increase (Fig. 3). The evolution of the deviatoric stresses in the overconsolidated case is also satisfactorily reproduced, while for the normally consolidated sample a strain softening after a peak strength is predicted, which is not observed in the experimental results. (Yu, 1998) also identified the same difference when modelling the test, showing that the absence of peak is not usual in the experimental undrained behaviour of normally consolidated clays. In any case, the difference between experimental and numerical behaviour obtained with Eqs. (18) and (20) is not associated with the effect of these equations. With both equations, p_R / p_0 values of nearly 1 are obtained when starting from initial conditions of both heavy overconsolidation (Fig. 6b) and normal consolidation (Fig. 6a). However, the latter case obtains the worst result with Eq. (18) in relative terms, which makes the improvement provided by Eq. (20) substantial. Thus, given the low computational cost increase of Eq. (20) with respect to Eq. (18) (which computes F), the use of Eq. (20) represents a step forward in the implementation of elastoplastic constitutive laws in implementation platforms.

4. Conclusions

In this work, the Current Increment Corrects Error (CICE) using the symbolic algebra to correct the potential integration drift has been proposed. The performance of CICE has been evaluated implementing the Clay and Sand Model (Yu, 1998) in COMSOL Multiphysics (Comsol AB, 2018). The results obtained by deriving the plastic multiplier from

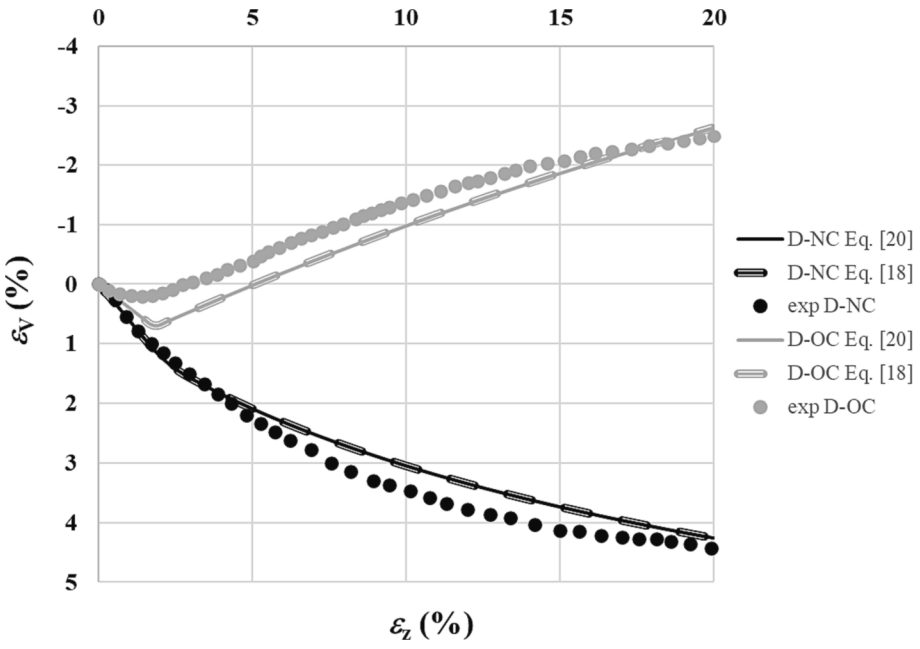

Fig. 2. Evolution of the axial strain ε_z and the volumetric strain ε_V in the drained tests. In black, normally consolidated sample. In grey, heavily overconsolidated sample. Markers, experimental data. Lines, model results.

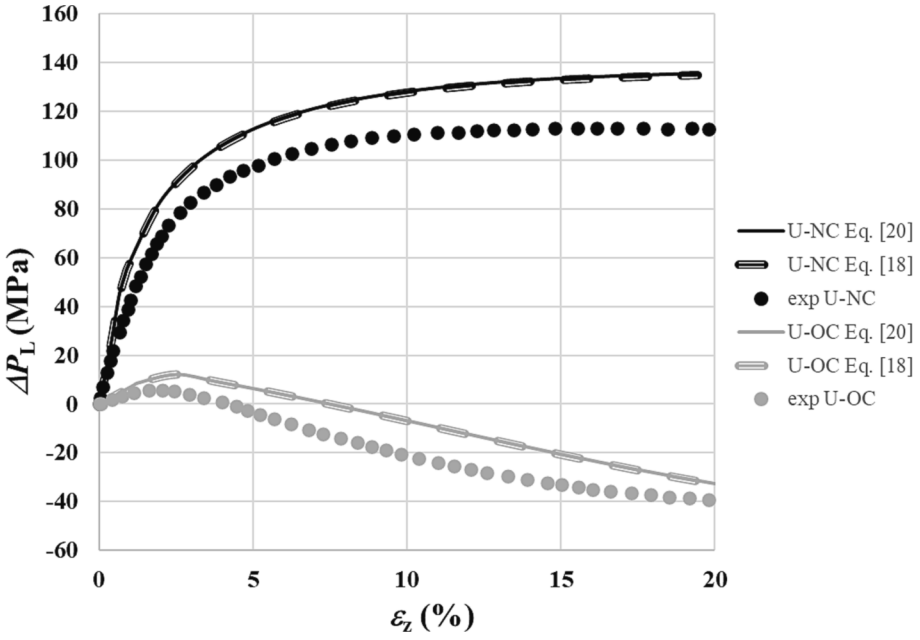

Fig. 3. Evolution of the axial strain ε_z and the water pressure increase ΔP_L in the undrained tests. In black, normally consolidated sample. In grey, heavily overconsolidated sample. Markers, experimental data. Lines, model results.

the consistency of the increment of the yield function F (i.e. $dF = 0$) are very similar to those obtained when deriving it from imposing the consistency of F (i.e. $F = 0$). However, with practically no increase in computational cost, the latter approach makes the plastic drift virtually zero, thus making it the recommended integration procedure.

CRediT authorship contribution statement

Vicente Navarro: Conceptualization, Methodology, Writing – original draft, Writing – review & editing, Funding acquisition, Supervision. **Arianna Pucci:** Conceptualization, Methodology, Formal analysis, Investigation, Writing – review & editing, Resources. **Erik Tengblad:** Methodology, Writing – original draft. **Francesca Casini:** Conceptualization, Writing – review & editing, Funding acquisition, Resources, Supervision. **Laura Asensio:** Writing – original draft, Writing – review & editing, Funding acquisition, Supervision.

Declaration of Competing Interest

The authors declare that they have no known competing financial interests or personal relationships that could have appeared to influence the work reported in this paper.

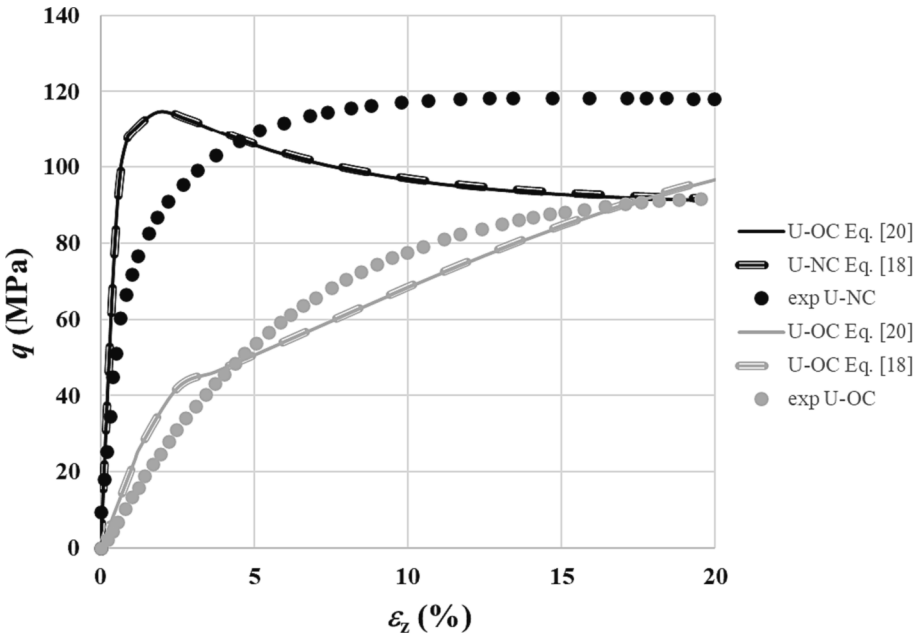

Fig. 4. Evolution of the axial strain ε_z and the von Mises stress q in the undrained tests. In black, normally consolidated sample. In grey, heavily overconsolidated sample. Markers, experimental data. Lines, model results.

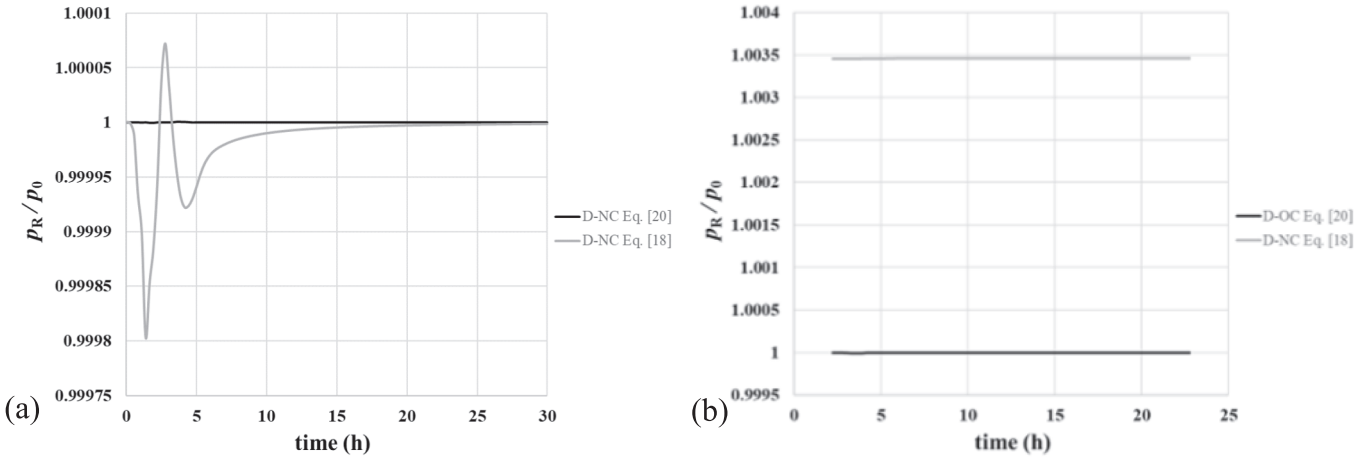

Fig. 5. Evolution of p_R / p_0 in the drained tests. (a) Normally consolidated sample. (b) Heavily overconsolidated sample.

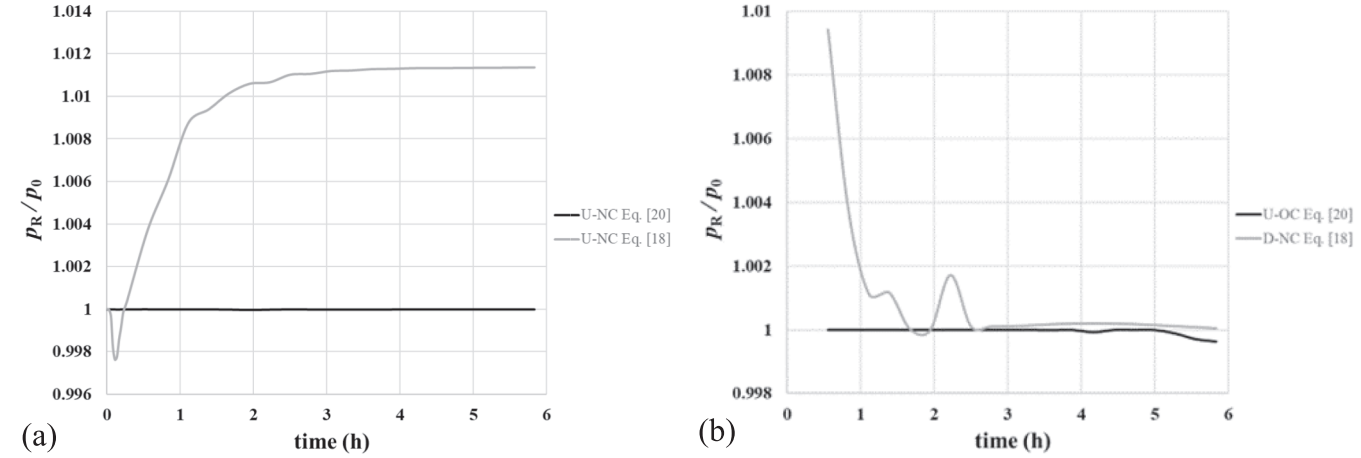

Fig. 6. Evolution of p_R / p_0 in the undrained tests. (a) Normally consolidated sample. (b) Heavily overconsolidated sample.

Data availability

The experimental information used has been obtained from the literature and is conveniently referenced and available for researchers to use.

Acknowledgements

This work is part of the project 2022-GRIN-34421, co-funded by Universidad de Castilla-La Mancha UCLM (15 %) and the European Regional Development Fund EDRF (85 %). The second author acknowledges the Ministerio dell'Università e della Ricerca for the financial support of her PhD fellowship through the PON/DM 1061 (10/08/2021).

References

Alonso, E.E., Gens, A., Josa, A., 1990. A constitutive model for partially saturated soils. Géotechnique. 40 (3), 405–430. https://doi.org/10.1680/geot.1990.40.3.405.

Alonso, E.E., Vaunat, J., Gens, A., 1999. Modelling the mechanical behaviour of expansive clays. Eng. Geol. 54, 173–183. https://doi.org/10.1016/S0013-7952(99)00079-4.

Bishop, A.W., Henkel, D.J., 1957. The Measurement of Soil Properties in the Triaxial Test. Edward Arnold Publishers Ltd, London.

Borja, R.I., Lee, S.R., 1990. Cam-Clay plasticity, Part 1: Implicit integration of elasto-plastic constitutive relations. Comput. Methods Appl. Mech. Eng. 78 (1), 49–72. https://doi.org/10.1016/0045-7825(90)90152-C.

Comsol AB (2018) Comsol Multiphysics Reference Manual. 5.3. COMSOL AB. https://doc.comsol.com/5.3/doc/com.comsol.help.comsol/COMSOL_ReferenceManual.pdf (accessed September 2023).

Gens, A., Alonso, E.E., 1992. A framework for the behaviour of unsaturated expansive clays. Can. Geotech. J. 29, 1013–1032. https://doi.org/10.1139/t92-120.

Gens, A., Potts, D.M., 1988. Critical state models in computational geomechanics. Eng. Comput. 5, 178–197. https://doi.org/10.1108/eb023736.

Gobbert, M.K., Churchill, A., Wang, G., Seidman, T.I. 2009. COMSOL Multiphysics for efficient solution of a transient reaction-diffusion system with fast reaction, in: Rao Y. (Ed.), Proceedings of the COMSOL Conference, Boston, 2009. https://www.comsol.com/paper/comsol-multiphysics-for-efficient-solution-of-a-transient-reaction-diffusion-sys-6309 (accessed September 2023).

Halilovič, M., Vrh, M., Štok, B., 2009. NICE—An explicit numerical scheme for efficient integration of nonlinear constitutive equations. Math. Comput. Simul 80, 294–313. https://doi.org/10.1016/j.matcom.2009.06.030.

Halilovič, M., Starman, B., Vrh, M., Stok, B., 2017. A robust explicit integration of elasto-plastic constitutive models, based on simple subincrement size estimation. Eng. Comput. 34 (6), 1774–1806. https://doi.org/10.1108/EC-03-2016-0103.

Lloret-Cabot, M., Sheng, D., 2022. Assessing the accuracy and efficiency of different order implicit and explicit integration schemes. Comput. Geotech. 141, 104531 https://doi.org/10.1016/j.compgeo.2021.104531.

Martins, J.R.R.A., Hwang, J.T., 2013. Review and unification of methods for computing derivatives of multidisciplinary computational model. AIAA J. 51 (11), 2582–2599. https://doi.org/10.2514/1.J052184.

Navarro, V., Yustres, Á., Asensio, L., De la Morena, G., González-Arteaga, J., Laurila, T., Pintado, X., 2017. Modelling of compacted bentonite swelling accounting for salinity effects. Eng. Geol. 223, 48–58. https://doi.org/10.1016/j.enggeo.2017.04.016.

Navarro, V., Asensio, L., Gharbieh, H., De la Morena, G., Pulkkanen, V.-M., 2019. Development of a multiphysics numerical solver for modeling the behavior of clay-based engineered barriers. Nuclear. Eng. Technol. 51, 1047e1059. https://doi.org/10.1016/j.net.2019.02.007.

Navarro, V., Cabrera, V., De la Morena, G., Asensio, L., Yustres, A., Torres-Serra, J., 2022. A new double-porosity macroscopic model of bentonite free swelling. Eng. Geol. 305, 106725 https://doi.org/10.1016/j.enggeo.2022.106725.

Navarro, V., Asensio, L., Cabrera, V., De la Morena, G., Yustres, A., 2023. Compacted bentonite hydro-mechanical modelling when interaggregate porosity tends to zero. Environ. Earth Sci. 82, 253. https://doi.org/10.1007/s12665-023-10936-w.

Potts, D.M., Gens, A., 1985. A critical assessment of methods of correcting for drift from the yield surface in elasto-plastic finite element analysis. Int. J. Numer. Anal. Meth. Geomech. vol. 9, n.o 2, 149–159. https://doi.org/10.1002/nag.1610090204.

Rowe, P.W. 1962 The Stress-Dilatancy Relation for Static Equilibrium of an Assembly of Particles in Contact. Proceedings of the Royal Society of London. Series A, Mathematical and Physical Sciences. 269, 1339, 500-527. https://doi.org/10.1098/rspa.1962.0193.

Vaunat, J., Cante, J.C., Ledesma, A., Gens, A., 2000. A stress point algorithm for an elastoplastic model in unsaturated soils. Int. J. Plast 16 (2), 121–141. https://doi.org/10.1016/S0749-6419(99)00033-9.

Yu, H.S., 1998. CASM: A unified state parameter model for clay and sand. Int. J. Numer. Anal. Meth. Geomech. 22 (8), 621–653. https://doi.org/10.1002/(SICI)1096-9853(199808)22:8<621::AID-NAG937>3.0.CO;2-8.